

**UNCLASSIFIED**

**AD 435740**

**DEFENSE DOCUMENTATION CENTER**

**FOR**

**SCIENTIFIC AND TECHNICAL INFORMATION**

**CAMERON STATION, ALEXANDRIA, VIRGINIA**



**UNCLASSIFIED**

**NOTICE:** When government or other drawings, specifications or other data are used for any purpose other than in connection with a definitely related government procurement operation, the U. S. Government thereby incurs no responsibility, nor any obligation whatsoever; and the fact that the Government may have formulated, furnished, or in any way supplied the said drawings, specifications, or other data is not to be regarded by implication or otherwise as in any manner licensing the holder or any other person or corporation, or conveying any rights or permission to manufacture, use or sell any patented invention that may in any way be related thereto.

435740

AD No.

DDC

FILE COPY

2-60-63-1

2-60-63-1 • SEPTEMBER • 1963

GAS DYNAMICS  
RR-9-63-14

1

TECHNICAL REPORT

HYPERSONIC CYLINDER WAKE STUDIES AT MACH 20

1963-14

435740



2-60-63-1 • SEPTEMBER • 1963

2-60-63-1

GAS DYNAMICS  
RR-9-63-14

TECHNICAL REPORT

## HYPERSONIC CYLINDER WAKE STUDIES AT MACH 20

by

A.C. BROWN

R.L. KRAMER

C.E. SMITH

*Lockheed*

**MISSILES & SPACE COMPANY**

A GROUP DIVISION OF LOCKHEED AIRCRAFT CORPORATION

SUNNYVALE, CALIFORNIA

## FOREWORD

The work described in this report is the first phase of an extensive study of hypersonic wakes and trails being conducted in the Physical Sciences Laboratory of Lockheed Missiles & Space Company (LMSC). This study is part of an effort in the gas dynamics area which is conducted under the general direction of Dr. Daniel Bershader, Senior Member.

The authors wish to acknowledge extensive contributions made by the following members of the hot-shot tunnel group: J. R. Heim who is in charge of the tunnel operation and who is assisted by I. N. Ingham, J. E. Franklin, and T. Wilcox; E. E. McAdams, Jr., who is responsible for the instrumentation and who is assisted by J. M. Cox, Sr. The authors further acknowledge the assistance of M. J. Lanfranco for the method-of-characteristics calculation, and W. G. Vincenti (consultant from Stanford University) for valuable discussions and suggestions.

This work is supported primarily by the Polaris reentry systems department of the Missile Systems Division, and partially by the LMSC Independent Research Program.

↓  
ABSTRACT

✓  
The initial phase in a study of the fluid mechanical behavior of wakes behind simple bodies is described ~~in this report.~~ Experimental measurements in both the viscous and the inviscid flow-fields of a two-dimensional circular-cylinder model were made in the LMSC hot-shot tunnel. The free-stream Reynolds number, based on model diameter, was varied between 1,800 and 90,000 at a nominal Mach number of 20.

Profiles of pitot pressure, which extended from the axis to the bow shock wave, were measured at four locations behind the model. Schlieren photographs of the bow and wake shock waves were taken. Calculations of the inviscid flow-field over the model were made by means of a method-of-characteristics program for comparison with experimental data. An embedded shock wave was inserted numerically in the flow field to simulate the wake shock-wave system.

The measured and computed profiles of pitot pressure in the inviscid regions of flow, as well as shock-wave shapes, are in good agreement. Details of the pitot-pressure distribution in the viscous wake are evident in the experimental data.

↑

## CONTENTS

Section	Page
Foreword	iii
Abstract	iv
Illustrations	vi
1 Introduction	1-1
2 Hot-Shot Tunnel Facility and Instrumentation	2-1
3 Data Reduction	3-1
4 Experimental Testing Conditions	4-1
5 Theoretical Model	5-1
6 Pitot-Pressure Distribution	6-1
7 Planned Future Work	7-1
8 References	8-1

## ILLUSTRATIONS

Figure		Page
2-1	Tunnel Schematic	2-2
2-2	Oscillograph Record, Run 782	2-4
2-3	Pitot Rake	2-5
2-4	Model and Rake in Test Section	2-7
4-1	Tunnel Mach-Number	4-4
4-2	Tunnel Shock-Wave Location	4-5
4-3	Repeatability of Lateral Pitot-Pressure Distribution (5 Diameters Behind Cylinder; Mach Number = 18 , Reynolds Number = 1800)	4-6
4-4	Schlieren Photograph, Cylinder at Mach Number 21	4-8
4-5	Variation of Measured Pitot-Pressure With Probe Reynolds Number	4-9
4-6	Calculated Reynolds-Number Ratio in Cylinder Wake	4-11
4-7	Effect of Viscous Correction on Lateral Pitot-Pressure Distribution (5 Diameters Behind Cylinder; Mach Number = 18 , Reynolds Number = 1800)	4-12
5-1	Circular Cylinder With Afterbody	5-2
5-2	Computed Surface-Pressure Distribution ( $M_{\infty} = 20$ , $\gamma = 1.4$ )	5-4
5-3	Shock-Wave Shapes for Flow Over Cylinder	5-6
6-1	Lateral Pitot-Pressure Distribution (2 Diameters Behind Cylinder)	6-2
6-2	Lateral Pitot-Pressure Distribution (3 Diameters Behind Cylinder)	6-3
6-3	Lateral Pitot-Pressure Distribution (5 Diameters Behind Cylinder)	6-4
6-4	Lateral Pitot-Pressure Distribution (8 Diameters Behind Cylinder)	6-5

Section 1  
INTRODUCTION

The wakes of reentry bodies are an important part of the problem of ballistic missile defense. A body entering the atmosphere deposits energy into the gases around and behind the body. The physical behavior of the total configuration of reentry-body and gas-flow environment is subject to detection, discrimination, and subsequent defensive action. Conversely, knowledge of the configuration forms the basis for the design of offensive systems with increased penetrability.

Numerous theoretical studies of the flow caused by reentry bodies have been made, but all of these studies are limited by the particular assumptions that were required to make the problem tractable. Feldman (Ref. 1) has considered the laminar wake in thermodynamic equilibrium, while Lees and Hromas (Ref. 2) treated the turbulent wake in equilibrium, and Lien, Erdos, and Pallone (Ref. 3) have investigated laminar and turbulent nonequilibrium wakes. Lees (Ref. 4) recently presented a summary of theoretical progress to which the reader is referred for a more complete description of the work that has been done.

Significant experimental work has been done both in the ballistic range and in the wind tunnel. Representative of the former are the works of Dana and Short (Ref. 5), Slattery and Clay (Ref. 6), and Pallone et al. (Ref. 7). Although reentry velocities and temperatures can be simulated in the ballistic range, detailed measurements in the flow field are extremely difficult to make. On the other hand, detailed mappings of flow fields are being accomplished in continuous wind tunnels, but they must be done at lower velocities and temperatures. McCarthy and Kubota (Ref. 8), Dewey (Ref. 9), and Kendall (Ref. 10) have measured various properties of wakes in continuous tunnels.

A number of theoretical and experimental studies of problems relating to reentry physics are in progress at LMSC. Since fluid mechanical behavior of wakes is fundamental to analysis of wake observability, measurements of the wake aerodynamics of simple bodies are being made in the LMSC hot-shot tunnel. Concurrent theoretical studies are being correlated with these experimental observations.

The initial phase of these wake studies is reported here. A two-dimensional model was chosen to ease the problem of making comparisons with theory, as well as to afford comparisons with the results in Refs. 8 and 9, at a lower Mach number. The method-of-characteristics, which was used to compute the flow field for the body, is simpler for plane flow than for axisymmetric flow and is used readily for bodies at an angle-of-attack. Furthermore, the viscous wake is thicker for axisymmetric flow and intrudes into the inviscid flow-field to a greater extent than with the two-dimensional case.

Secondary advantages of two-dimensional models are the elimination of support interference, improved flow visualization, and the simplicity of instrumentation alignment behind the model.

The results of theoretical and experimental investigations of the flow past a circular cylinder at about Mach 20 are described in this report. The theoretical analysis is confined to solutions for the inviscid flow-field, computed with the method-of-characteristics. These solutions are then compared both to experimental measurements of pitot pressure in the wake of the model and to schlieren photographs of the flow. The large Reynolds-number range of the hot-shot tunnel, which is one of the tunnel's most significant attributes, is utilized fully in this series of experiments.

Research will continue on the effects of model cross-sectional shape upon the wake fluid mechanics. Some work will be done with three-dimensional models and considerable effort will be devoted to development of the instrumentation which will provide more information on the gas properties.

## Section 2 HOT-SHOT TUNNEL FACILITY AND INSTRUMENTATION

### 2.1 TUNNEL FEATURES

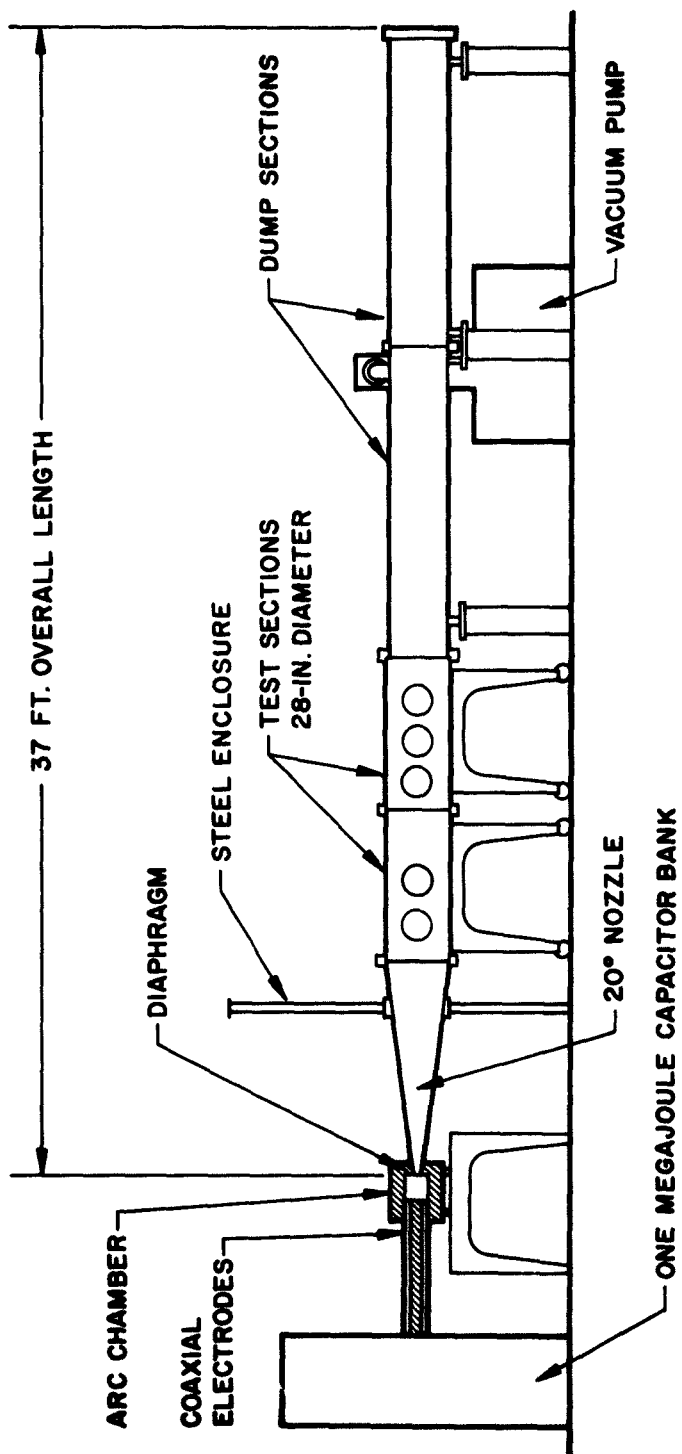
The experimental study of wakes is being conducted in the LMSC hot-shot tunnel. In this tunnel, there is an elongated test section with optical viewing ports, and wake-study instrumentation supports are available for a distance of up to 8 ft behind a model.

A schematic drawing of the hot-shot tunnel appears in Fig. 2-1. The electric arc discharge, which heats the gas confined in the arc chamber, can be established with air or nitrogen at densities of 1 to 110 amagats. The arc discharge duration is approximately 70  $\mu$ sec. Available throat inserts range in size from 0.050 to 0.300-in. in diameter, with corresponding geometrical expansion ratios to the 28-in. diameter test section from  $3.1 \times 10^5$  to  $8.7 \times 10^3$ . A choice of throat size, gas density, and energy input allows testing in Mach-number and Reynolds-number ranges of approximately 12 to 36 and  $2 \times 10^3$  to  $2 \times 10^6$  per ft.

Starting transients in the conical nozzle last from 5 to 7 milliseconds (ms) before quasi-steady flow is established. A minimum of 20 ms of useful run time is available in the test section after the starting transients have passed. With the 41-cu in. volume of the arc chamber and a 0.2-in. diameter throat, as were used in this wake study, the pressure drop-off in the chamber is approximately 3 percent per ms.

### 2.2 GENERAL INSTRUMENTATION

Instrumentation used in this study includes a single-pass schlieren system using 12-in. diameter parabolic mirrors with focal lengths of 10 ft.



2-2

LOCKHEED MISSILES &amp; SPACE COMPANY

Fig. 2-1 Tunnel Schematic

Pressures are measured in the arc chamber with full-bridge strain-gage transducers. Test-section pressures are measured with variable reluctance transducers similar to those developed at Arnold Engineering Development Center (Ref. 11). The nominal range of transducers is either 1/2 or 3 psi, depending on diaphragm thickness. These transducers (each with the inlet pressure-tube 1/16-in. inside diameter and approximately 2 in. in length) respond to a step change of pressure in approximately 1 ms.

The arc-chamber and test-section pressure transducers are driven and the return signals are amplified by C.E.C. 20-kc carrier amplifiers. The amplified signals are in turn fed to a recording oscillograph equipped with galvanometers in which the response is down 3 db at 440 cps. An example of an oscillograph record of the arc-chamber and test-section pressures is shown in Fig. 2-2.

The pressure measurement system is calibrated statically before each run. In most cases, the linearity and repeatability of the calibration are within  $\pm 2$  percent. In practice, the pressure data on a tunnel run tend to scatter somewhat more than this, but seldom as much as  $\pm 5$  percent. On all pressure measurements of primary importance such as the arc-chamber pressure and the model stagnation-point pressure (which is used for normalizing the wake pitot pressures), two transducers are used to increase the reliability of the measurements.

### 2.3 MODEL AND PITOT-PRESSURE RAKE

The two-dimensional model used for the wake study is a 1-in. diameter rod which spans the test section and which is supported at both ends outside the flow region. Two pressure transducers are mounted in the model to record the stagnation pressure on the centerline of the tunnel.

A pitot-pressure rake, shown in Fig. 2-3, permits simultaneous pitot-pressure measurements at a number of points along a line which is perpendicular to the tunnel and model axes at a certain distance behind the model.

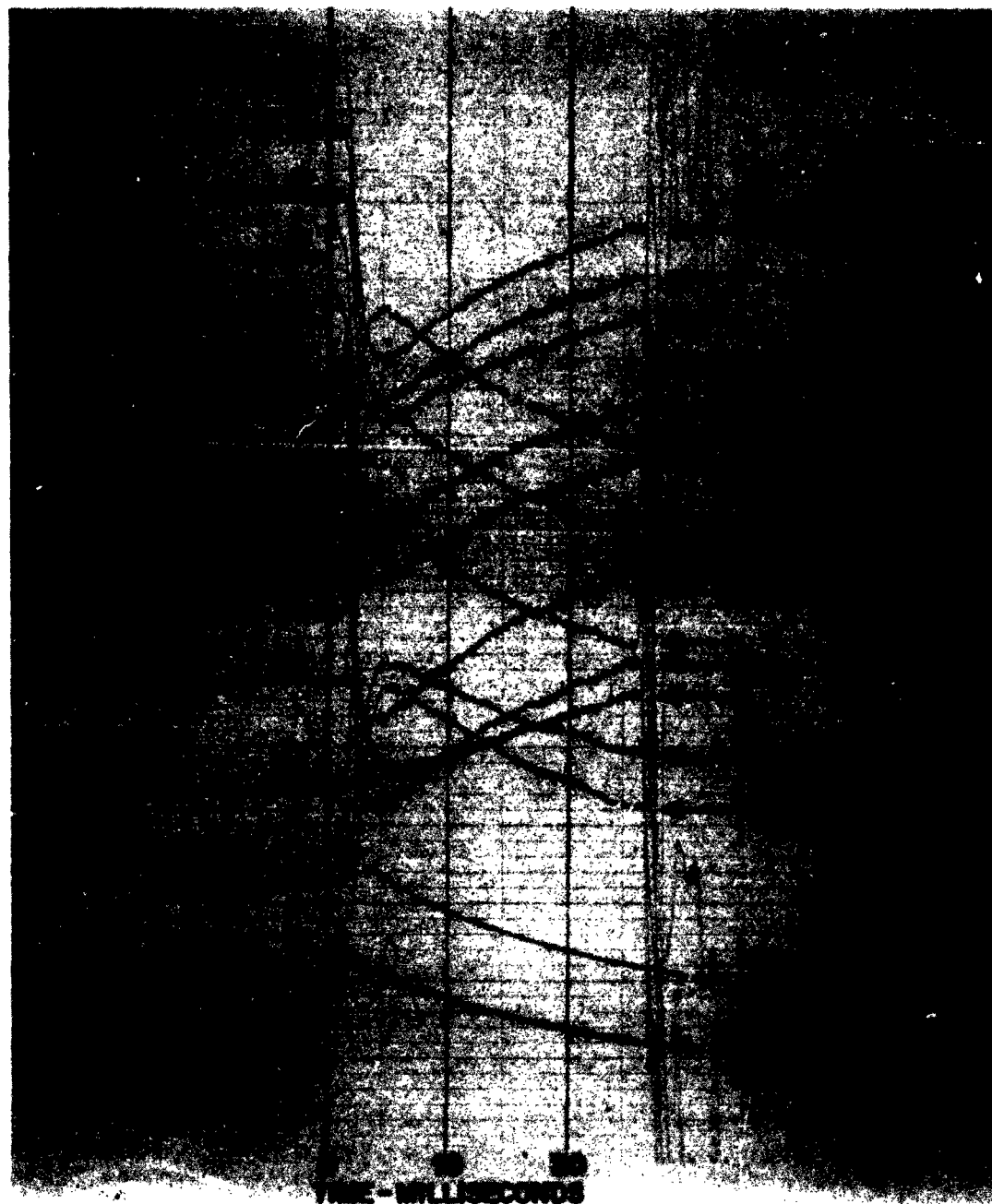


Fig. 2-2 Oscillograph Record, Run 782

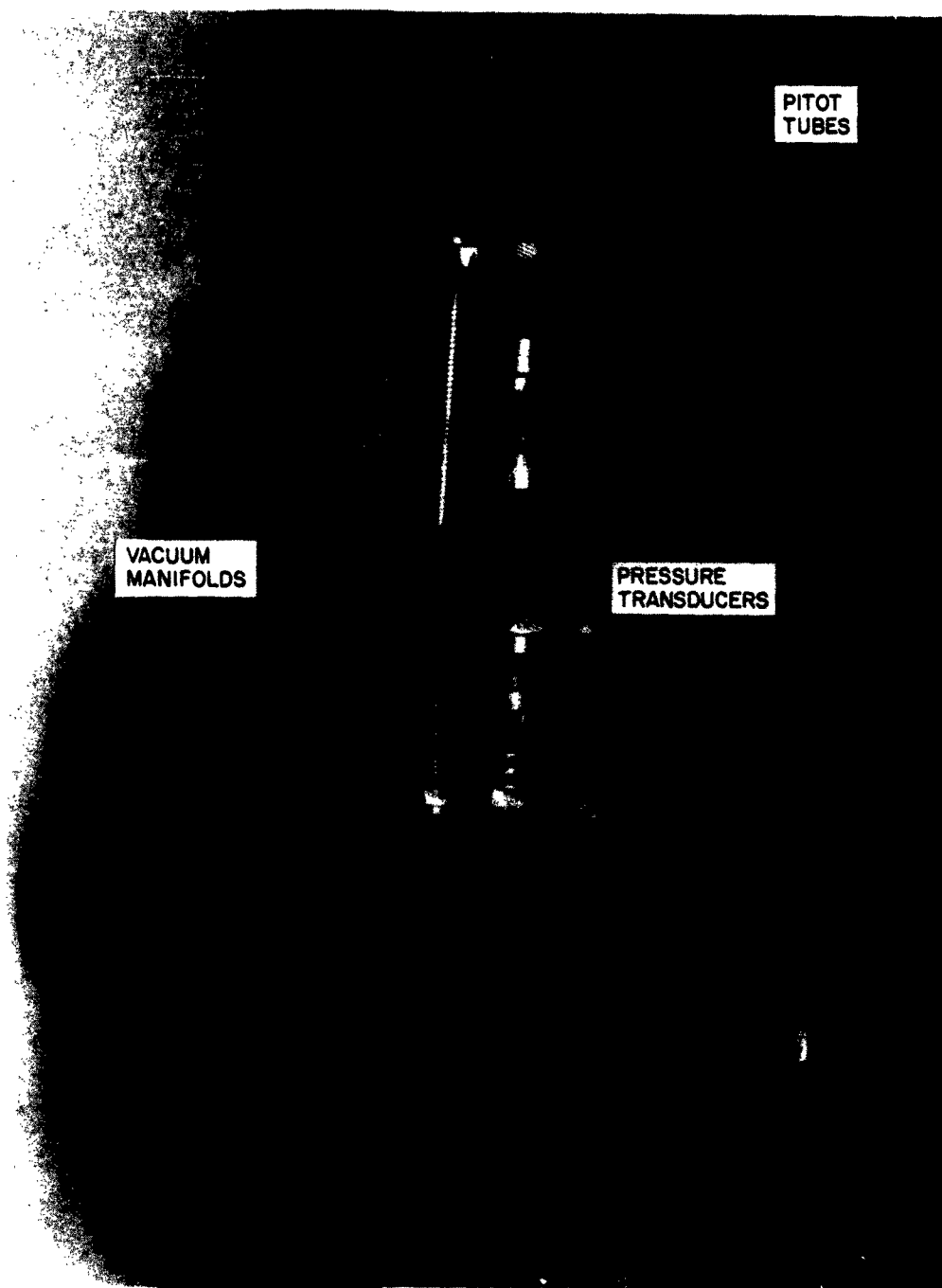


Fig. 2-3 Pitot Rake

The rake consists of a housing in which the transducers are stacked and connected to pitot tubes leading out through the 24-deg half-angle leading edge of the housing. The transducers are disc shaped, 0.18 in. thick, and approximately 3/4 in. in diameter. These transducers are stacked and connected with flexible tubes to the pitot tubes which are spaced over part of the rake width at 1/8-in. (center-to-center) distances. The pitot tubes are made from 0.092-in. o.d., 0.062-in. i.d., steel tubing which is flattened at the inlet end in the direction of the pressure gradients to approximately 0.08-in. o.d.

A photograph of the model and rake placement in the tunnel appears in Fig. 2-4. Measurements were made on only one side of the model centerline since early tests indicated that the flow is symmetrical. This arrangement allowed maximum spatial coverage and resolution with the 11 transducers. Pitot-pressure measurements were made with the rake at four axial stations, 2, 3, 5, and 8 diameters behind the model centerline. Complete lateral coverage from the model axis to a point outside the bow shock was obtained for each axial station. At each position of the rake, tests were made at the three operating conditions described in subsection 4.1.



Fig. 2-4 Model and Rake in Test Section

### Section 3 DATA REDUCTION

Flow conditions in the test section are calculated by means of a digital computer program. Thermodynamic properties of equilibrium molecular nitrogen (Ref. 12) are used with both the measured arc-chamber pressure and the model stagnation-point pressure to calculate flow variables at 5-ms intervals during the test. Intermolecular force (van der Waals) effects are included because of the high densities that exist in the arc chamber.

The gas density in the arc chamber at any given instant is computed by subtracting the integrated mass-flow through a choked throat from the initial mass. One-dimensional quasi-steady adiabatic flow is assumed to exist in the nozzle at each instant (a delay is incorporated to reflect the time it takes for the gas to go down the nozzle). The hypersonic approximation is made that almost all (99.5 percent) of the stagnation enthalpy is converted into velocity in the test section. The effective area ratio is computed for a uniformly distributed mass flow at the model location.

Section 4  
EXPERIMENTAL TESTING CONDITIONS

4.1 REYNOLDS-NUMBER VARIATION

The experiments have been conducted at three discrete operating conditions, which were chosen to produce a significant spread in Reynolds number within the limitations of both facility and instrumentation. Less significant variations in other flow parameters occurred as a consequence.

The throat diameter was unchanged at 0.200 in., which gave about the same area ratio for each test, with boundary-layer differences accounting for minor variations. High Reynolds numbers were obtained by operating with the highest initial pressure readily available from bottled gas. Since the stagnation temperature was moderate, the gas flow in the test section was super-cooled. At the lowest tested Reynolds number, the initial density was lower by a factor of 15, and the stagnation temperature was increased to about 4,500° K. At this condition, real gas effects were significant.

The test conditions were as follows:

Initial Pressure in Arc Chamber (psi)	Energy Added to Gas (kilojoules)	Stagnation Temperature (°K)	Reynolds Number per foot (ft <sup>-1</sup> )	Mach Number
1815	115	1600	10 <sup>6</sup>	21
615	105	3200	1.4 x 10 <sup>5</sup>	19
135	34	4500	2 x 10 <sup>4</sup>	18

The Mach number decreases with the Reynolds number because of the decrease in effective area ratio caused by the nozzle boundary-layer, and also the decrease in  $\gamma$  (specific heat ratio) as the temperature increases.

#### 4.2 TEST GAS

Nitrogen was used as the test gas. Nitrogen appears to cause less arc-chamber and throat erosion than air, and, more importantly, it behaves more nearly as a perfect diatomic gas over a wide temperature range. This latter point is significant when comparisons are made with simplified theories.

#### 4.3 MACH-NUMBER GRADIENT

Since the nozzle is conical, the test-section flow is not uniform. Although the velocity is practically constant, the Mach number increases as the gas stream expands. A simplified relationship between Mach number and pitot pressure for isentropic expansion of an ideal gas can be derived as follows:

$$M = \frac{v}{a} \sim \frac{v}{T^{1/2}} \sim \frac{v}{\rho^{1/2}}$$

where

- v = velocity
- a = speed of sound
- T = temperature
- $\rho$  = density
- $\gamma$  = ratio of specific heats

The pitot pressure,  $p$ , is approximately proportional to  $\rho v^2$  at hypersonic speeds. Consequently, when the gas moves from one test-section station to another at constant

velocity, the Mach number change is given by

$$\frac{M_2}{M_1} = \left(\frac{\rho_1}{\rho_2}\right)^{\frac{\gamma-1}{2}} = \left(\frac{p_1}{p_2}\right)^{\frac{\gamma-1}{2}} \text{ for } v_1 = v_2$$

Noting also that  $\rho_1 A_1 = \rho_2 A_2$ , where  $A$  is the cross-sectional area of the flow at the station denoted by the subscript, we have  $p_2/p_1 = A_1/A_2$ .

Measurements of free-stream pitot pressures have been made at several axial stations, and at different Reynolds numbers. The exploration was not comprehensive, but there are sufficient data to show that the Mach-number gradient is about one per ft at the highest Reynolds number. The gradient decreases as the tunnel boundary-layer thickness increases at the lower Reynolds numbers. This phenomenon is illustrated in Fig. 4-1.

#### 4.4 AVAILABLE TEST REGION

A shock wave is generated by the junction of the test section and the conical nozzle, as shown in Fig. 4-2. A calculation was made of the interaction between this shock wave and the bow shock wave from the model. Because of the high Mach number ahead of the intersection, the tunnel-wall shock wave is bent away from the tunnel axis rather than towards it, as would be the case at lower Mach numbers. Measurements of the tunnel shock-wave position have been made using a pitot-pressure rake at several axial stations. The results of these experiments, which define the available test section, are also shown in Fig. 4-2.

#### 4.5 QUALITY OF DATA

The repeatability of the pressure measurements is shown in Fig. 4-3. At the lowest Reynolds number, pitot pressures are lowest and therefore the measurements are

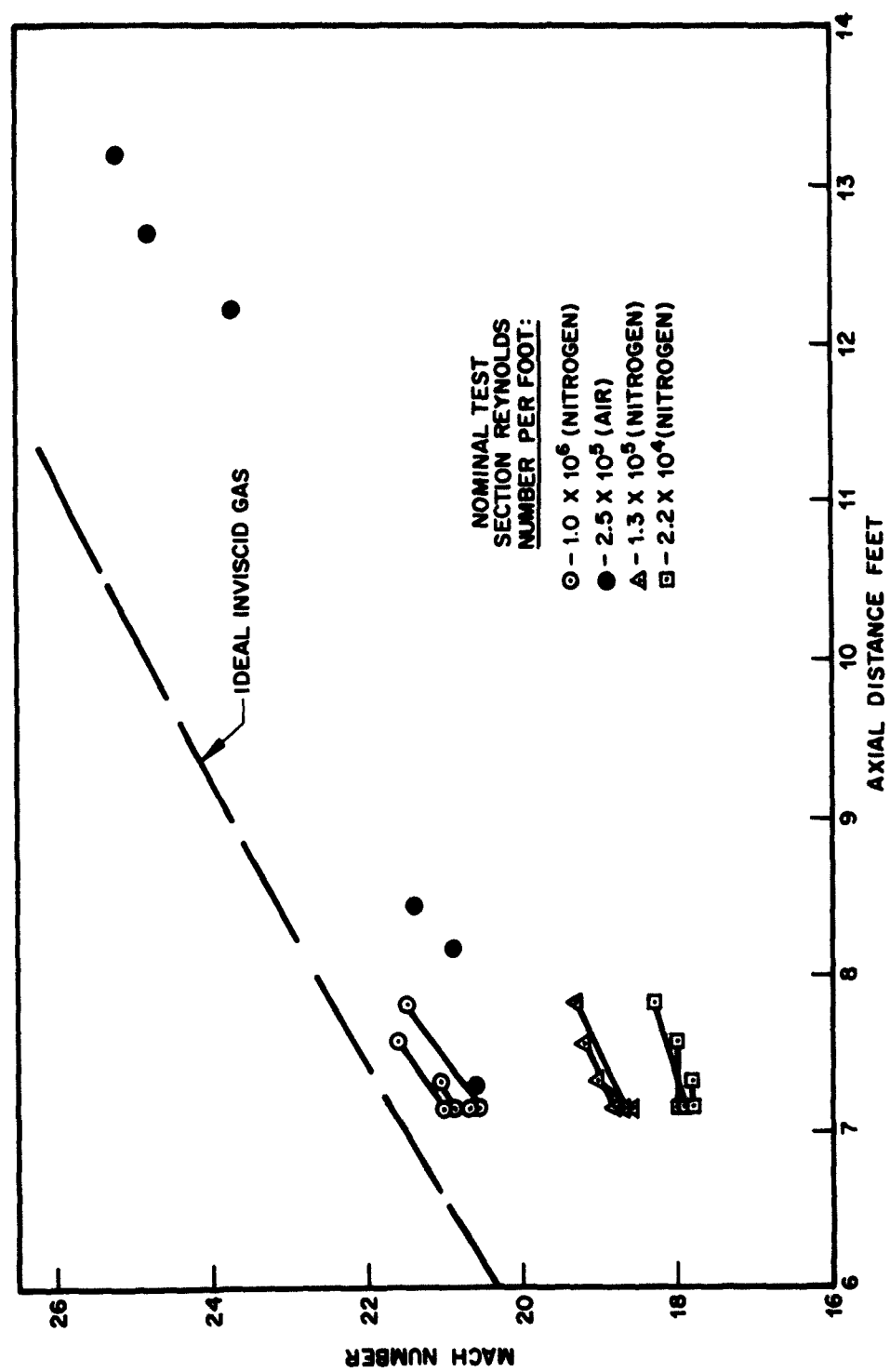


Fig. 4-1 Tunnel Mach-Number Gradient

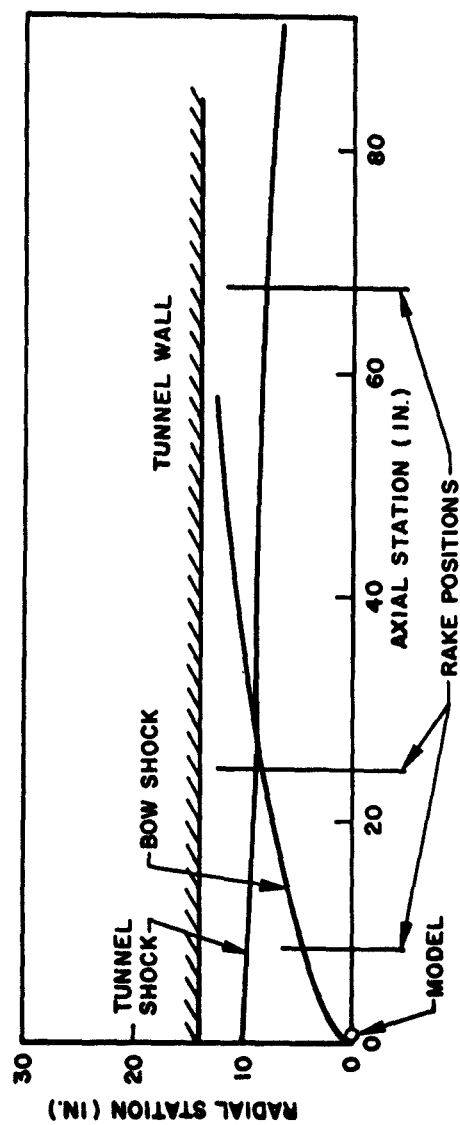


Fig. 4-2 Tunnel Shock-Wave Location

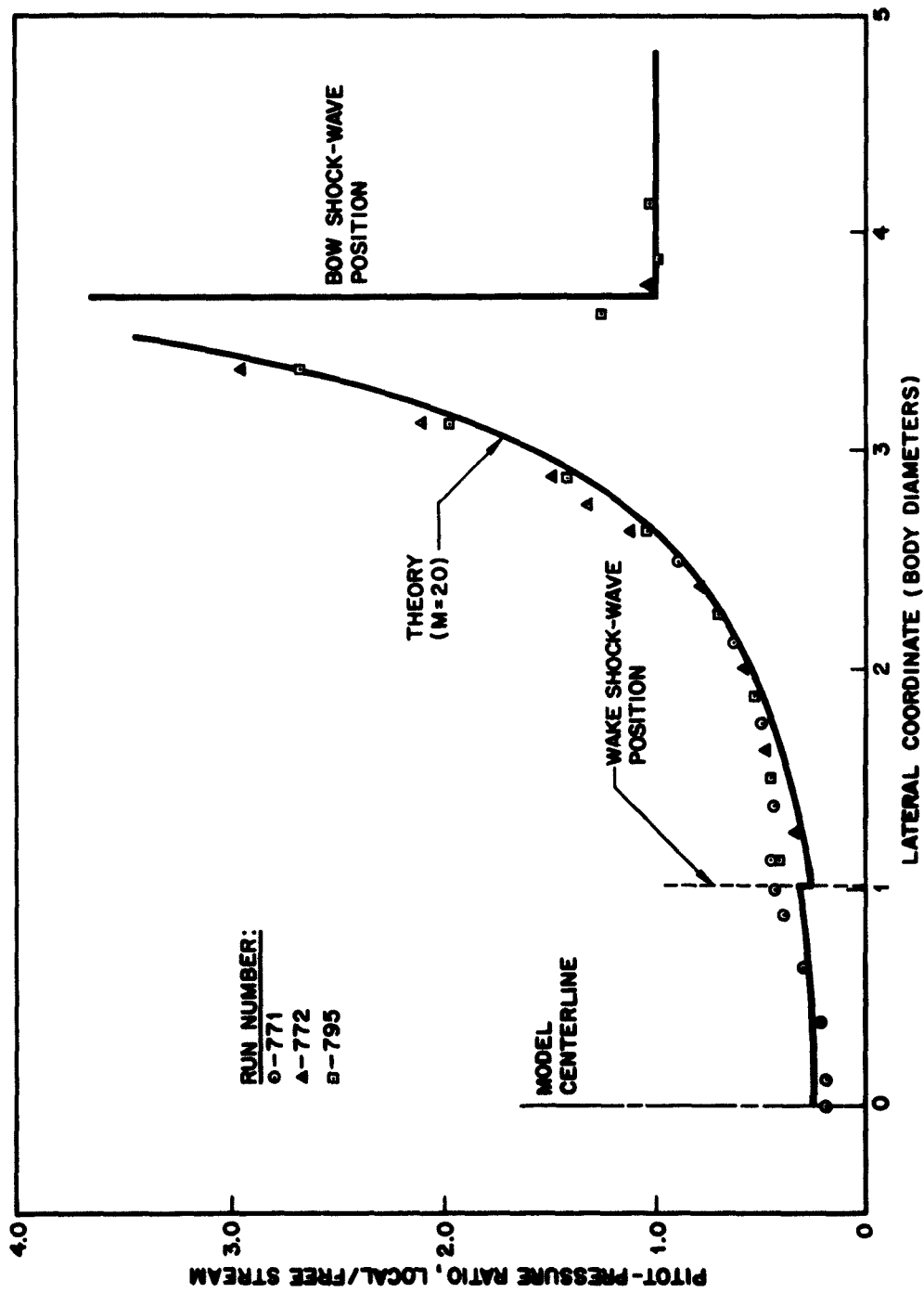


Fig. 4-3 Repeatability of Lateral Pitot-Pressure Distribution  
 (5 Diameters Behind Cylinder; Mach Number = 18, Reynolds Number = 1800)

least accurate. Three overlapping tests were made with the rake mounted 5 diameters behind the model. Although pressures as low as 0.02 psi are involved, it is difficult to distinguish in Fig. 4-3 between the results of one test and another.

Occasionally a pitot-pressure measurement fell out of line with others, as seen in Fig. 4-3. When this occurred, an explanation usually could be found in faulty behavior of the transducer or amplifier equipment; no such measurements were discarded unless an explanation could be found. Disagreements among supposedly good data are not large, and conclusions may be reached by averaging the measurements.

Schlieren photographs of the wake were taken during every run. At the highest Reynolds number, the bow shock-wave and wake shock-waves are clearly visible, and evidence of the viscous wake can be seen on some photographs. One of the best photographs is shown in Fig. 4-4. This probably represents the limit of what can be achieved in the facility with conventional schlieren techniques. At lower Reynolds numbers, only the bow shock-wave may be seen.

#### 4.6 LOW REYNOLDS-NUMBER EFFECTS ON PITOT-PRESSURE MEASUREMENT

It has been shown by various investigators that the measured pitot pressure deviates from the inviscid value when the Reynolds number, based on the probe diameter, falls below some limiting value. Much of the data which have been obtained are summarized in Ref. 13. A graph of pressure correction against Reynolds number is given in that reference. Although the data from several facilities are included, it is difficult to draw conclusions about the secondary effects of Mach number and stagnation temperature. Consequently, a mean line has been drawn and is used for pitot-pressure correction in this report, as shown in Fig. 4-5.

The local Reynolds number in the wake of a hypersonic blunt body is considerably smaller than the value in the free stream ahead of the body. An estimate of the Reynolds-number ratio along the wake axis (in terms of the free-stream Mach number)



Fig. 4-4 Schlieren Photograph, Cylinder at Mach Number 21

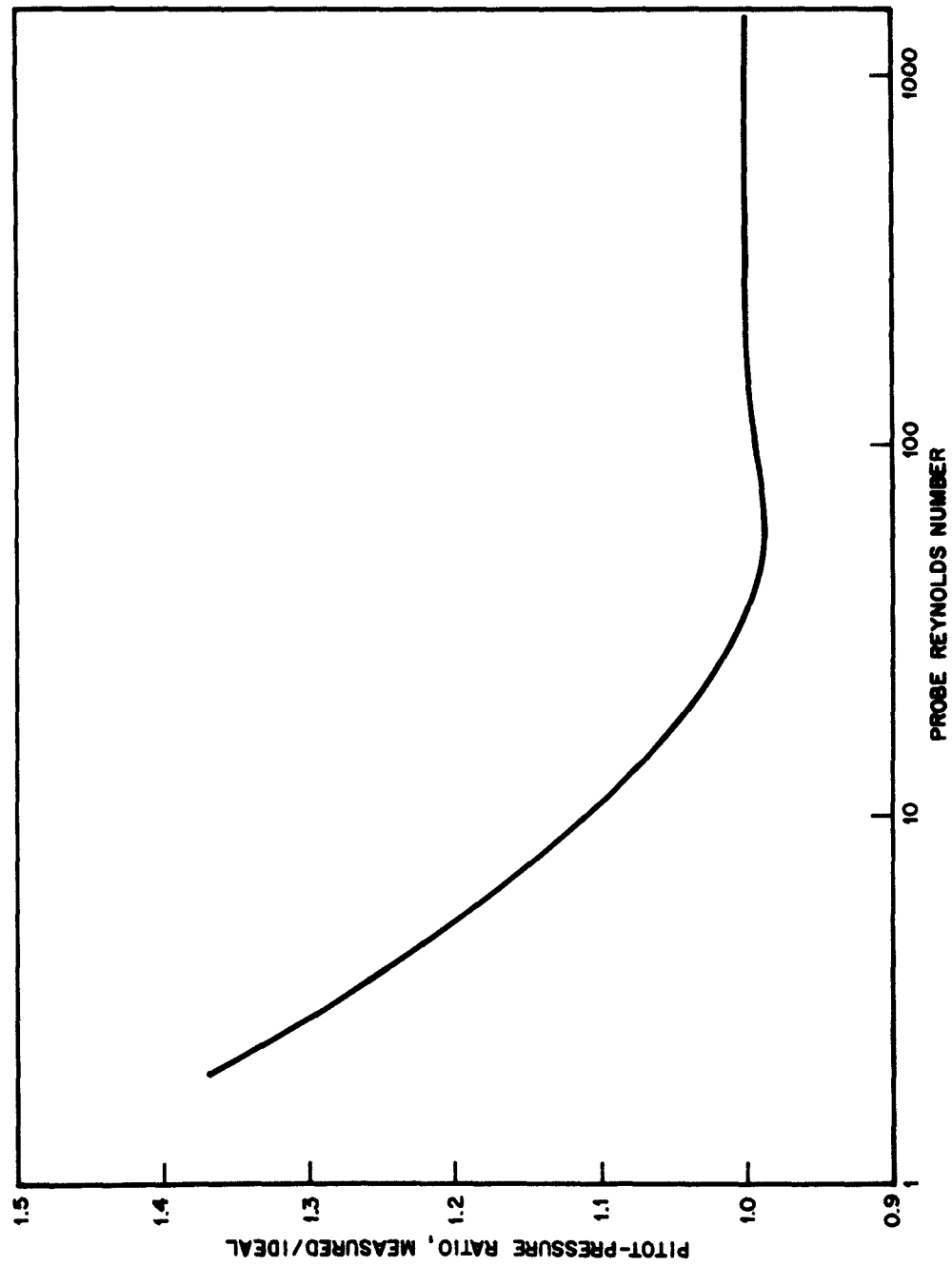


Fig. 4-5 Variation of Measured Pitot-Pressure  
With Probe Reynolds Number

may be obtained from blast-wave theory (Ref. 14), but it is not valid for extreme distances behind the body. The entropy rise through the shock wave is known in terms of the Mach number, and the axial pressure distribution is known in terms of the body-drag coefficient, Mach number, and specific heat ratio. To simplify the results, the isentropic relationship and the state equation for a perfect gas may be used with a power-law dependence of viscosity on temperature. The ratio of local Reynolds number per ft,  $Re$ , to the free-stream value,  $(Re)_{\infty}$ , for a cylinder then becomes

$$\frac{Re}{(Re)_{\infty}} = \frac{5.6}{(M_{\infty})^{1.26}} \left(\frac{x}{d}\right)^{-0.35}$$

where  $\left(\frac{x}{d}\right)$  is the axial distance downstream from the model (in model diameters). Demetriades (Ref. 15) has arrived at the same inverse dependence on the Mach number from experimental data of the transition from laminar to turbulent flow.

Although blast-wave theory is useful for predicting trends, it is generally not quantitatively accurate. Since the method-of-characteristics solution had been computed for the two-dimensional cylinder, it was used to obtain profiles of the Reynolds-number ratio at the four measurement stations. Again, a power-law temperature-viscosity relationship was assumed for simplicity. The results of this calculation are shown in Fig. 4-6. No correction was made for conditions in the viscous wake.

The pitot-pressure correction for each tube was calculated for all tests from the Reynolds number, based on tube height, with the aid of the data in Figs. 4-5 and 4-6. The viscous effect is most severe at the lowest free-stream Reynolds number. The results of the correction which was applied to data at 5 diameters downstream from the model for the lowest Reynolds number are shown in Fig. 4-7. The correction tends to move the data nearer to the theoretical prediction which is described in the next section.

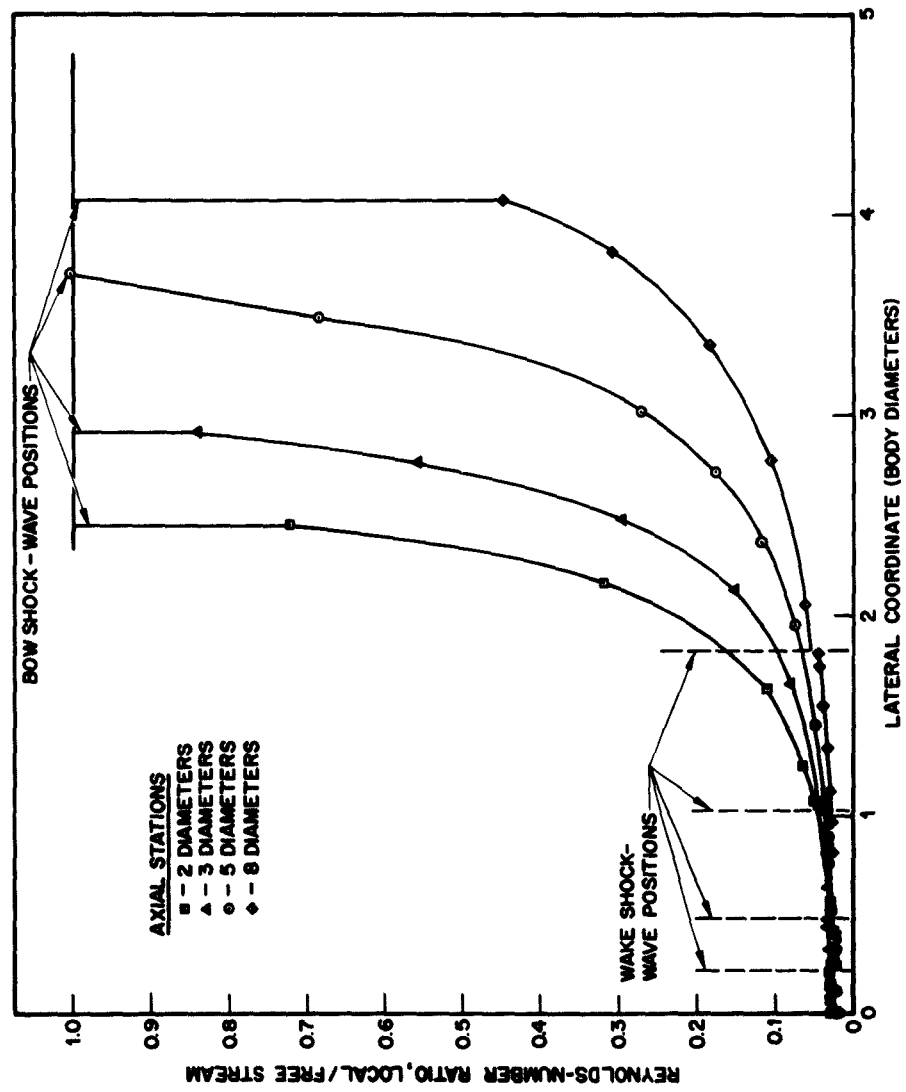


Fig. 4-6 Calculated Reynolds-Number Ratio in Cylinder Wake

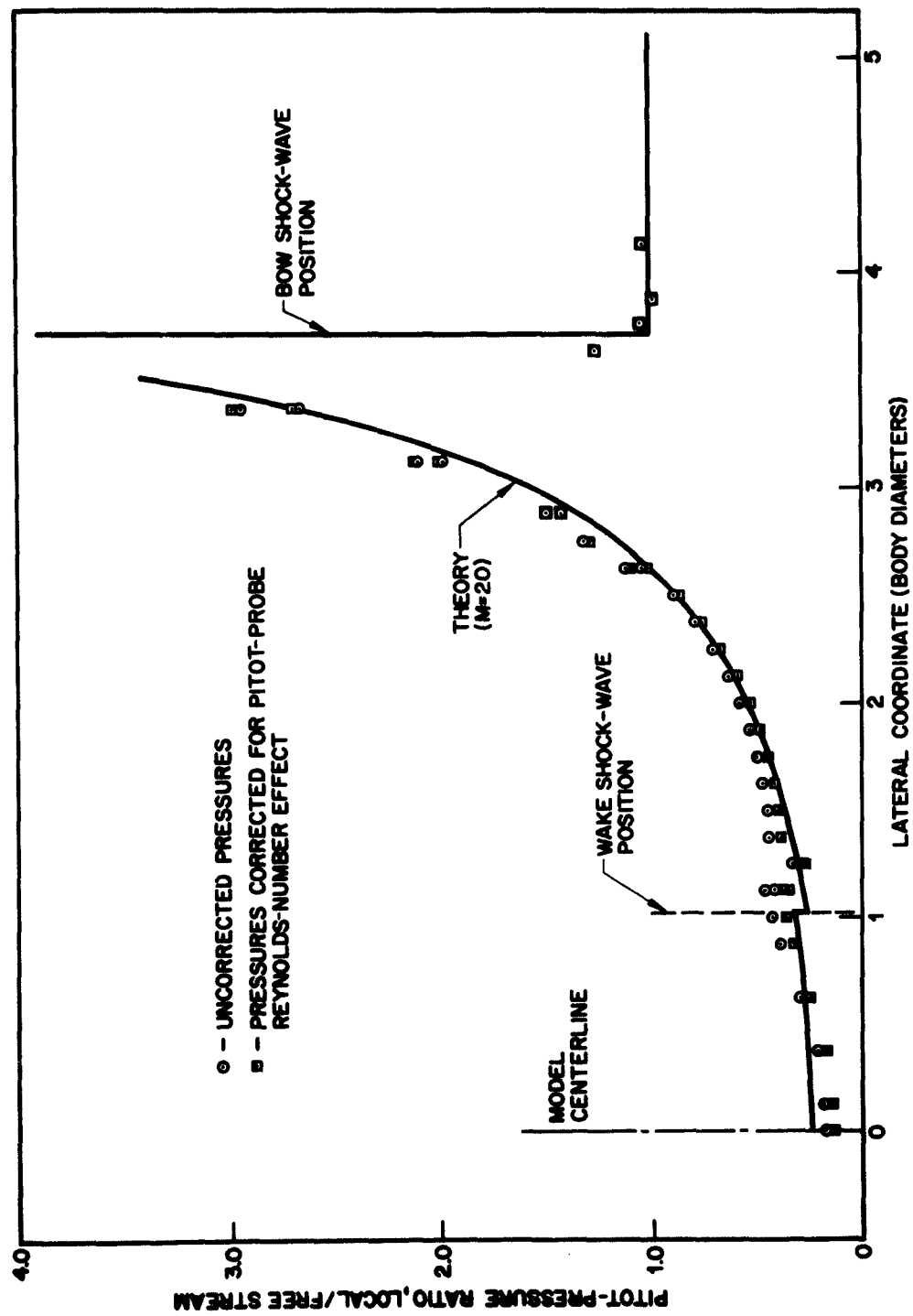


Fig. 4-7 Effect of Viscous Correction on Lateral Pitot-Pressure Distribution (5 Diameters Behind Cylinder; Mach Number = 18, Reynolds Number = 1800)

## Section 5 THEORETICAL MODEL

### 5.1 INVISCID FLOW-FIELD CALCULATION

The inviscid flow-field of a circular-cylinder body was calculated by means of a digital computer program which is based on the method of characteristics for an ideal gas. While this program requires a solid boundary (i.e., free-stream lines cannot be allowed), it does allow considerable geometric latitude. The program can compute flow fields which have embedded shock waves, if the waves start from the solid boundary at a finite compressive corner. Envelope shock waves (which start as a result of continuous compression) and intersecting shock waves cannot be handled by the program.

The flow-variable values at the starting line needed by the method-of-characteristics program were generated by another computer program, based on the work of Van Dyke (Ref. 16) and Fuller (Ref. 17). The method is an inverse one in which the shock-wave shape is specified, and the equations of motion are integrated from the shock until the body is located. At a free-stream Mach number of 20, a parabolic shock wave yields a body (for two-dimensional flow) that deviates from a constant radius by only 0.3 percent.

Since the computer program does not permit separated flow, it was necessary to replace the separated-flow region that exists behind a circular cylinder in a hypersonic flow with an equivalent solid-body shape. For the initial calculation, the complete model was taken to be a cylinder, joined tangentially to a wedge-shaped afterbody (see Fig. 5-1). This body shape neglects the lip shock-wave since it implies that the boundary layer separates tangentially.

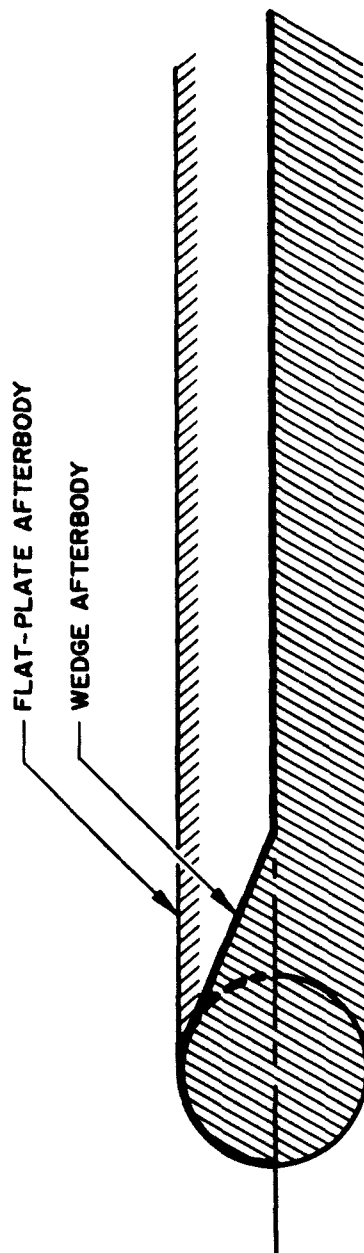


Fig. 5-1 Circular Cylinder With Afterbody

It also implies that the free shear-layer has no curvature from the point of separation to the axis. A trailing shock wave, originating at the apex of the assumed afterbody, turns the flow parallel to the axis. The displacement effects of the boundary layer (on the body) and the viscous wake (behind the trailing shock wave) were not accounted for in the calculations.

Calculations of the flow field for an ideal gas were performed with a free-stream Mach number of 20 and  $\gamma$  of 1.4. Solutions were obtained for the following three values of wedge afterbody half-angle: 26, 20, and 0 deg (the latter being a flat plate with a circular leading edge). The values of the pertinent flow variables were interpolated at axial locations of 2, 3, 5, and 8 diameters for comparison with experimental measurements. These calculations correspond to the case of an infinite free-stream Reynolds number and, consequently, represent a basic solution that would be modified slightly by the inclusion of displacement effects of the boundary layer and wake.

The 20-deg wedge model represents the first approximation to the free-shear-layer angle. The solution for this model was compared with the schlieren photographs, and a 26-deg wedge model was chosen as a second approximation. The computed origin of the trailing shock wave, as well as its subsequent path, is in reasonable agreement with the schlieren photographs at the high-Reynolds-number condition. An improvement in body shape, such as taking a slightly smaller angle on the free shear-layer and inserting a displacement thickness caused by the viscous wake, necessitates a new calculation for each Reynolds number.

Figure 5-2 shows the computed values of surface pressure for various body shapes. The pressure distribution along a flat plate with a circular leading edge corresponds within about 10 percent to the predictions of blast-wave theory. The pressure behind the wake shock wave is not influenced strongly by the choice of the angle of the free shear-layer. For the case of both 20 and 26 deg, the pressure returns nearly to the flat-plate value behind this shock wave. In addition, the surface pressure of the

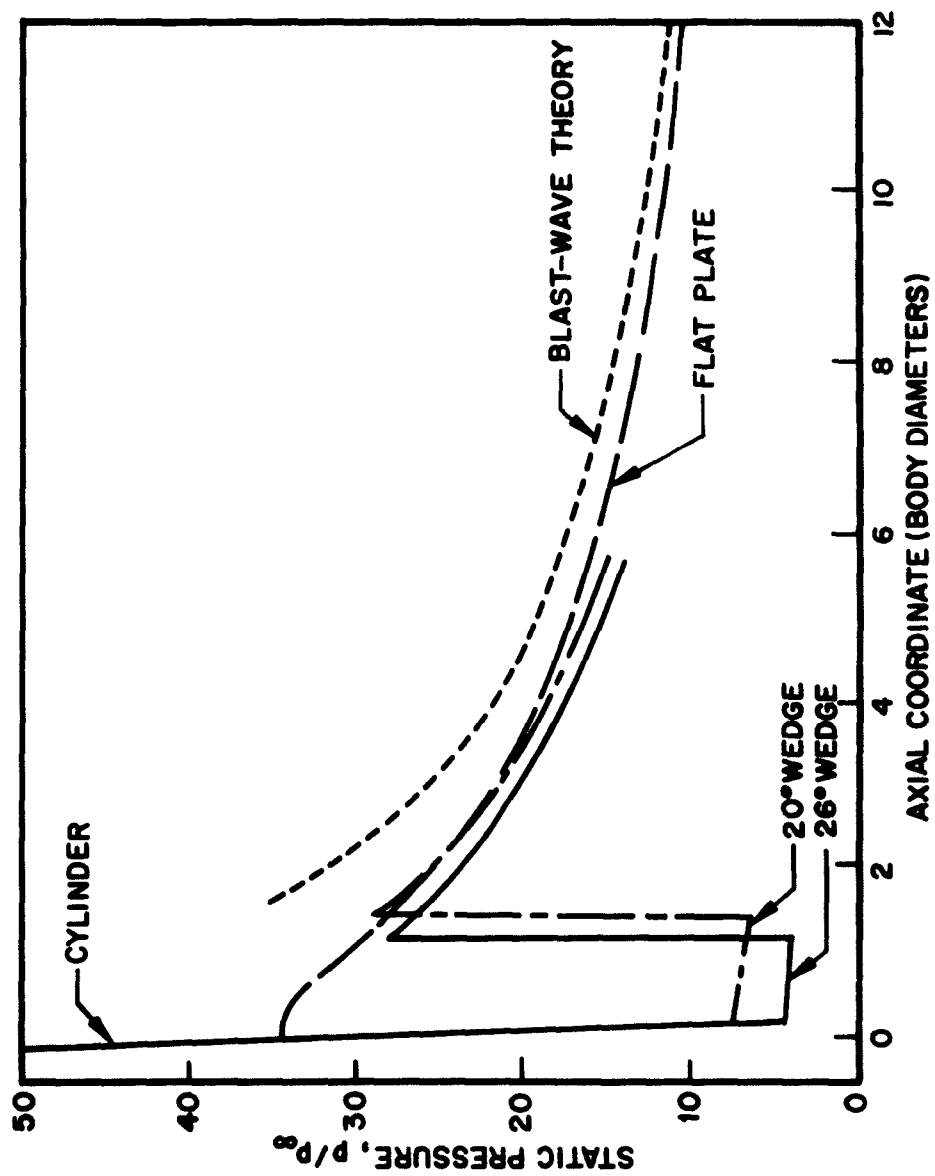


Fig. 5-2 Computed Surface-Pressure Distribution ( $M_\infty = 20$ ;  $\gamma = 1.4$ )

wedge-shaped afterbody is practically a constant, which justifies an approximation of the free shear-layer by a straight line.

## 5.2 COMPUTED SHOCK-WAVE SHAPES AND DISCUSSION

In the calculations, the shape of the bow shock wave depended only on the shape of the front portion of the cylindrical body, since a characteristic line from anywhere behind the 90-deg position of the cylinder did not intersect the shock wave. Inouye and Lomax (Ref. 18) reported a similar result for axisymmetric flow from calculations with hemisphere-cylinder bodies. Consequently, the choice of angle of the free-shear layer had no effect on the computed shape of the bow shock wave.

The computed bow shock-wave shape, and wake shock-wave shape for the 26-deg wedge afterbody, are shown in Fig. 5-3. Shock-wave position, as measured from schlieren photographs, is included for each of the three test conditions. The wake shock wave was visible only at the high Reynolds-number condition. In Fig. 5-3, the bow shock wave may be seen to move slightly toward the body as the Reynolds number decreases (or as the stagnation temperature increases).

The correlation between the computed and measured shape is surprisingly good, considering the sensitivity of the shock-wave shape to free-stream conditions. The tests were performed in a nozzle with a cone half-angle of 10 deg, while the calculations employed a uniform, parallel free-stream. Meyer (Ref. 19) used a perturbation of blast-wave theory, and showed that the bow shock wave moves farther from the body with source flow in the free-stream than it does with parallel flow.

The conical flow effect is not as large as expected, however, for two reasons. The first is that a certain amount of contouring of the nozzle is done by the boundary layer, and the effective cone angle is less than 10 deg. In particular, the thick boundary layer at the low Reynolds number causes nearly uniform flow in the test section (see Fig. 4-1).

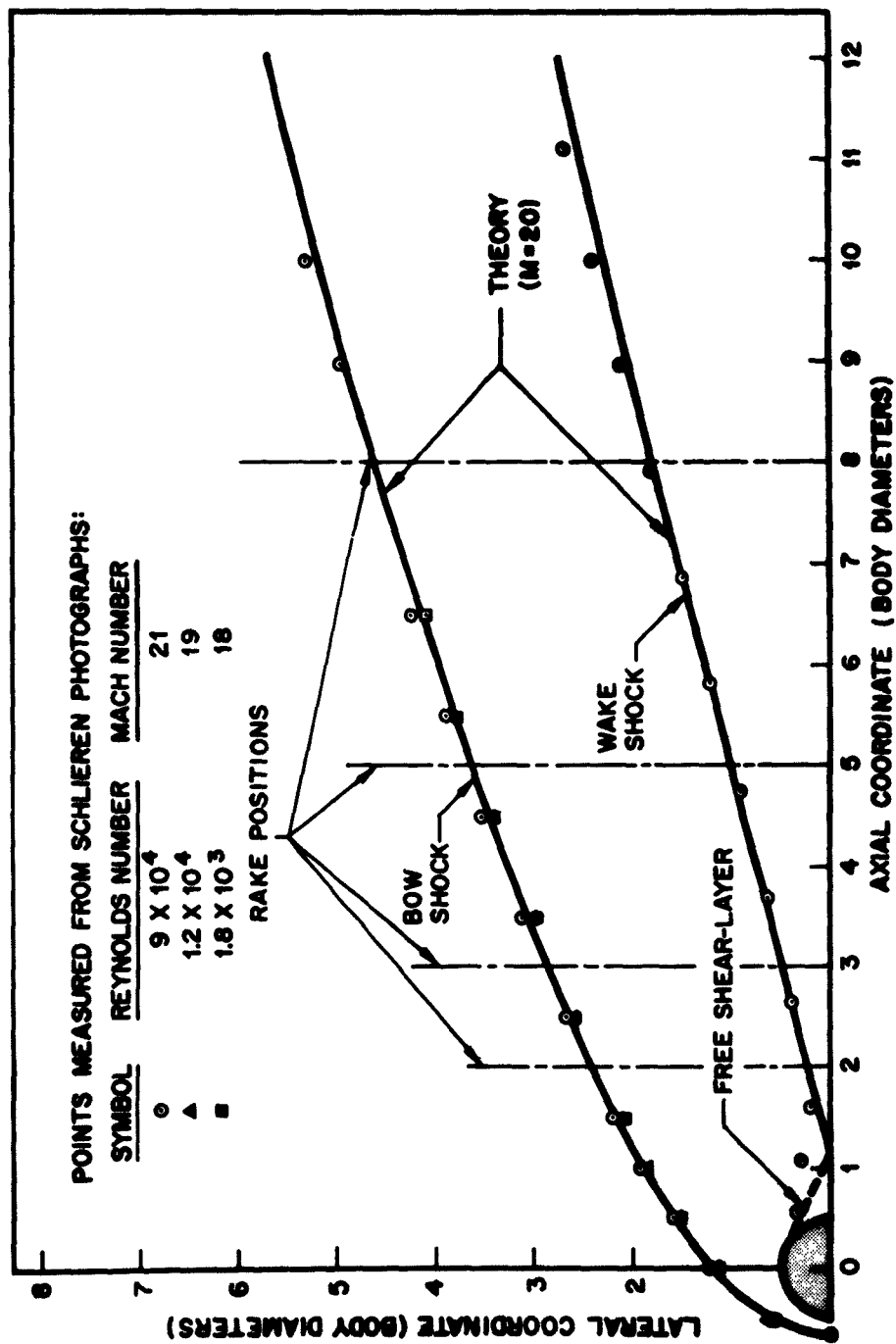


Fig. 5-3 Shock-Wave Shapes for Flow Over Cylinder

Secondly, the value of  $\gamma$  decreases as temperature increases, because of the excited state of the vibrational degrees of freedom. A reduction of the value of  $\gamma$  causes the bow shock wave to move closer to the body in accordance with the analysis of Chernyi (Ref. 14), which is based on the blast-wave analogy. As expected, the effect is observed to be largest at the lowest Reynolds number. Apparently, the effects of conical flow and reduced  $\gamma$  combine to yield a bow shock wave that corresponds to the shape computed for a parallel free-stream with a  $\gamma$  of 1.4.

The wake shock-wave system may be seen in the schlieren photograph (Fig. 4-4). The system consists of a lip shock wave which starts where the boundary layer separates from the body and which is joined by a trailing shock wave emanating from the wake neck. In the calculations, the lip shock wave is ignored, and the wake shock wave begins at the wake neck. Despite this simplification, a good agreement is obtained between the computed and observed shapes of the wake shock wave. In addition, the choice of an angle for the free shear-layer fixes only the origin of the wake shock wave. Its subsequent path depends on the calculation of the flow field, and cannot be influenced strongly by the location of its origin.

Section 6  
PITOT-PRESSURE DISTRIBUTION

Pitot pressures were computed by using the method-of-characteristics program (as described in Section 5) with the 26-deg wedge afterbody model. Comparisons of calculated and measured pitot-pressure profiles at axial locations of 2, 3, 5, and 8 diameters are presented in Figs. 6-1 through 6-4. The measured pressures are corrected for the low Reynolds-number effects discussed in paragraph 4.6, and are normalized with respect to the model stagnation-point pressure. The rake positions are shown in Fig. 5-3.

The general agreement between the experimental and calculated profiles is good. There are, however, several interesting points to be discussed. At the centerline, there is a dip in the profile which is due to the viscous wake. Near the body (2 diameters) the profile has a pronounced dip, while at the last axial station (8 diameters) the dip is quite shallow. At the highest Reynolds number, the viscous wake (corresponding to the dip) is narrow. The wake broadens as the Reynolds number is reduced until, at the lowest Reynolds number, the pitot pressure is less than the calculated inviscid value in the entire region between the wake shock waves. Although the pitot-tube spacing is not close enough to define the position of the wake shock wave accurately, it appears that this shock wave moves out slightly with decreasing Reynolds number. All of these observations are consistent with an inverse dependence of wake displacement thickness on the Reynolds number.

The wake shock wave appears to vanish at the lowest Reynolds number. However, since the flow must be bent back toward the free-stream direction, this result cannot be taken completely at its face value. There are at least two feasible explanations for the observed behavior. One is that the thicker wake cannot sustain a very strong

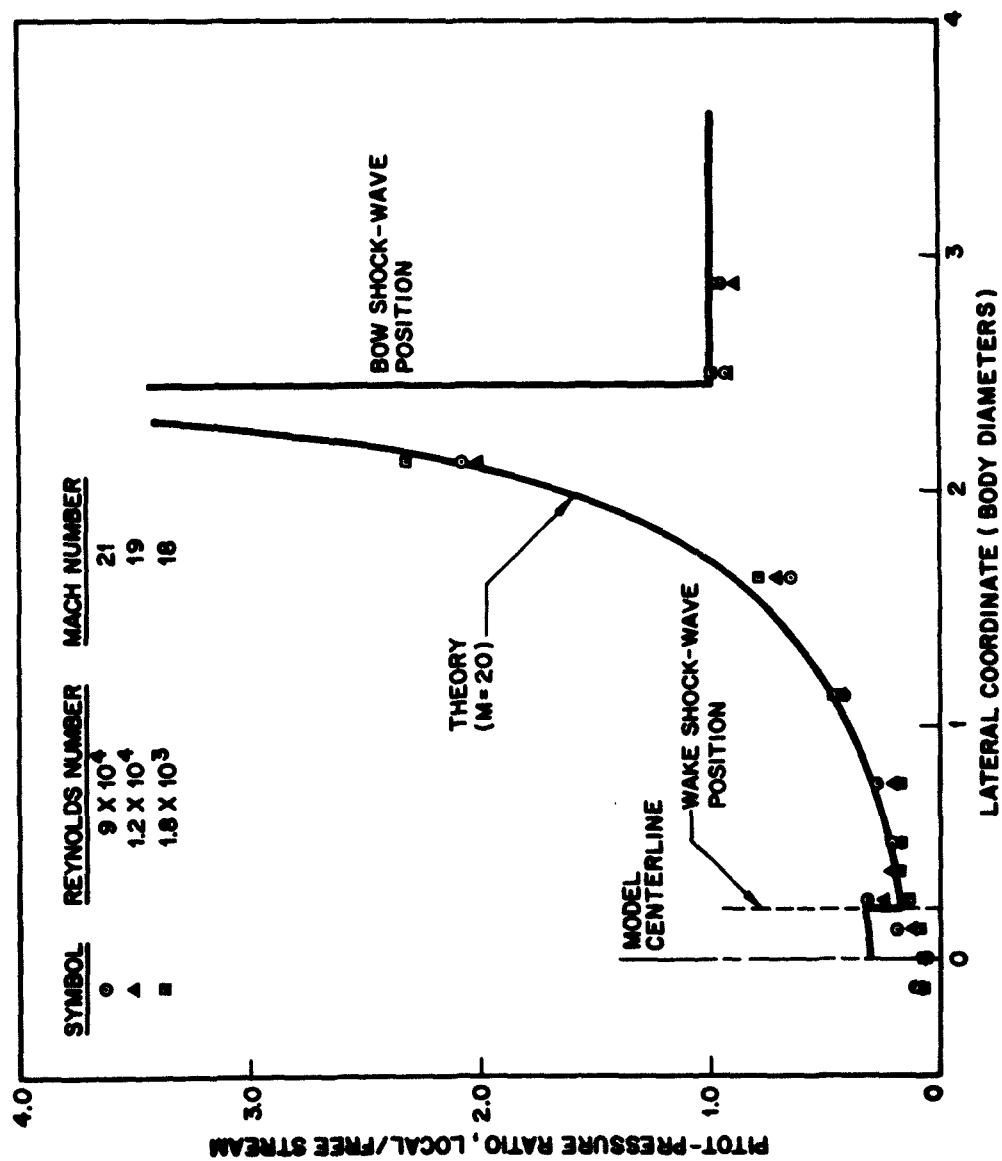


Fig. 6-1 Lateral Pitot-Pressure Distribution (2 Diameters Behind Cylinder)

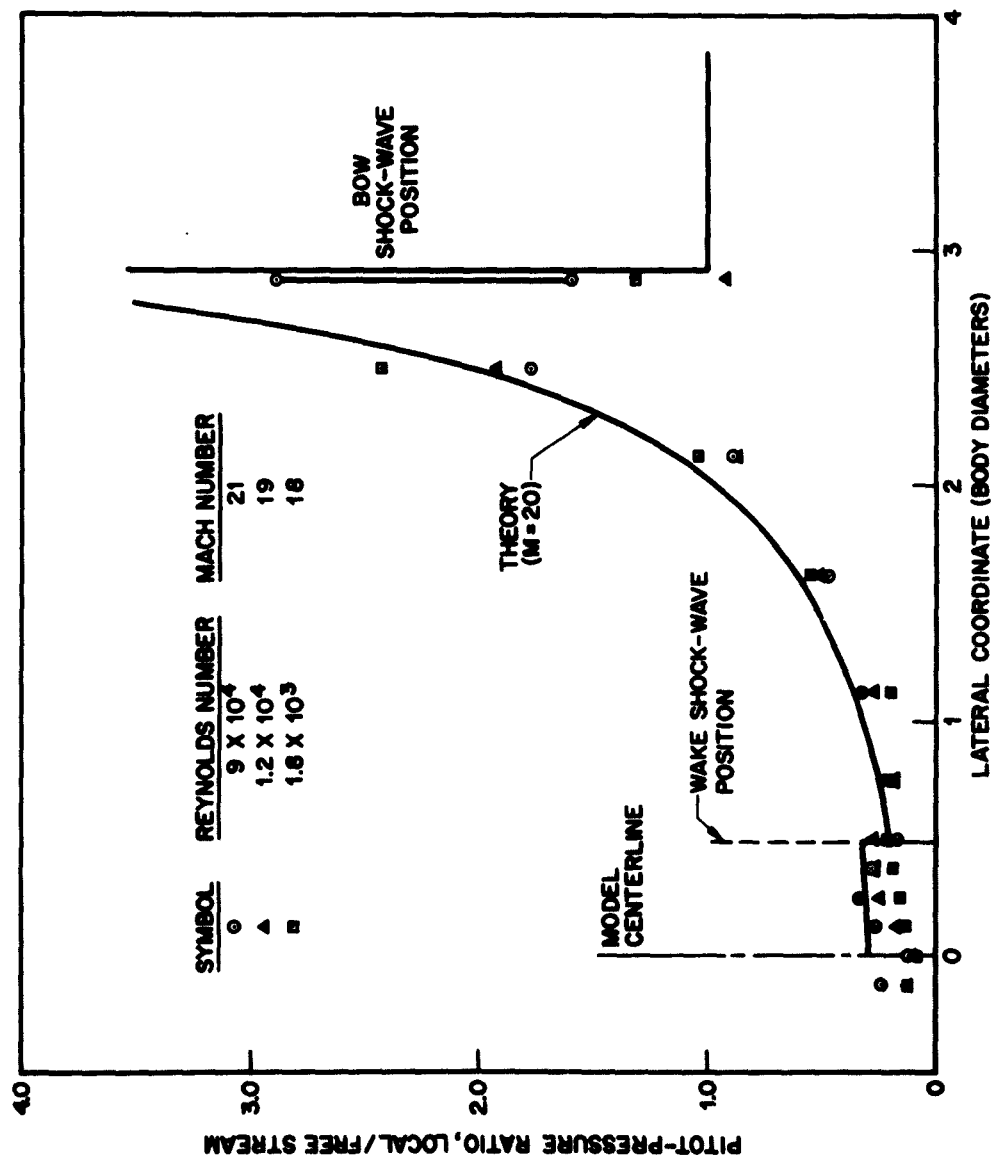


Fig. 6-2 Lateral Pitot-Pressure Distribution (3 Diameters Behind Cylinder)

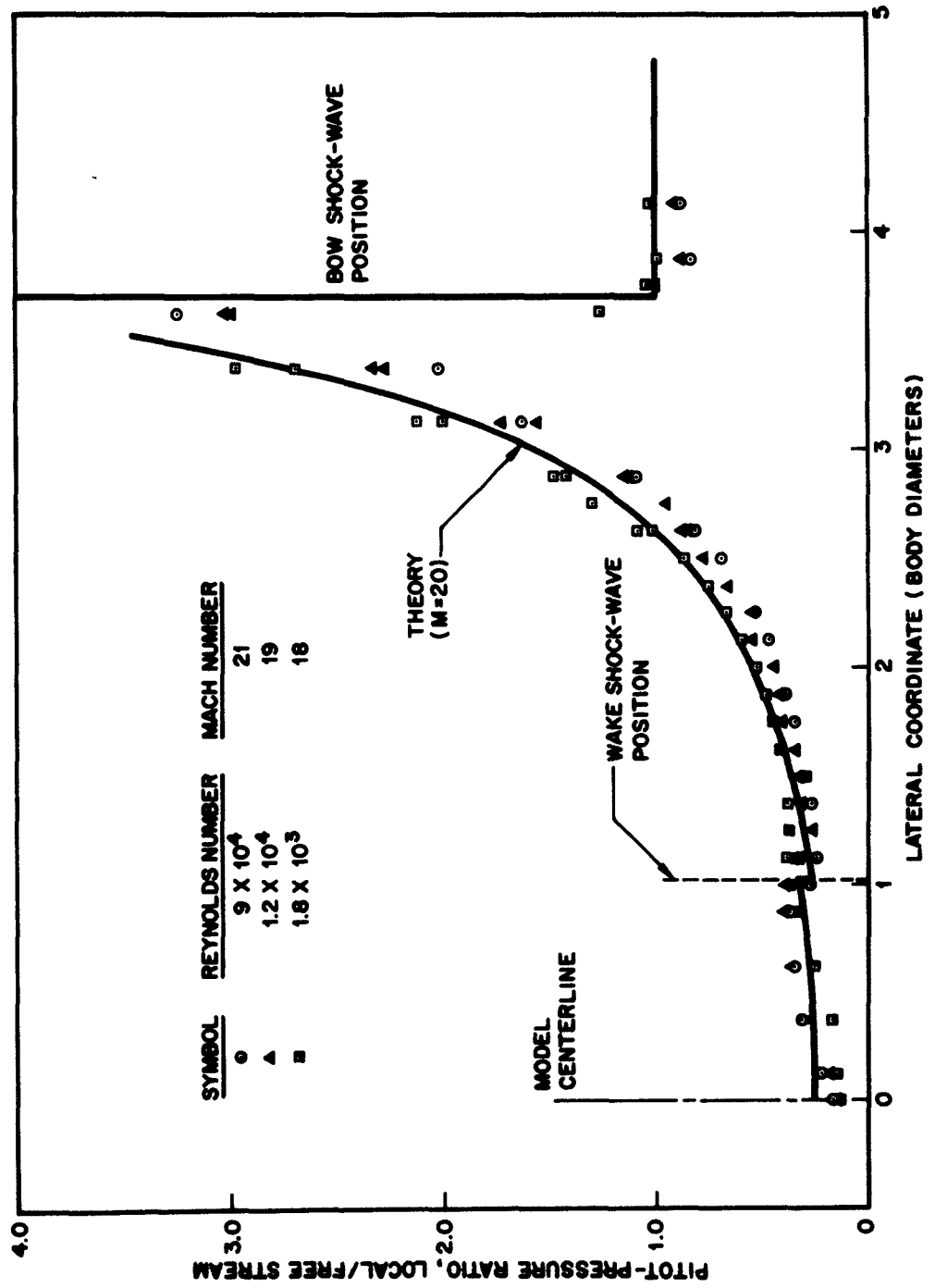


Fig. 6-3 Lateral Pitot-Pressure Distribution (5 Diameters Behind Cylinder)

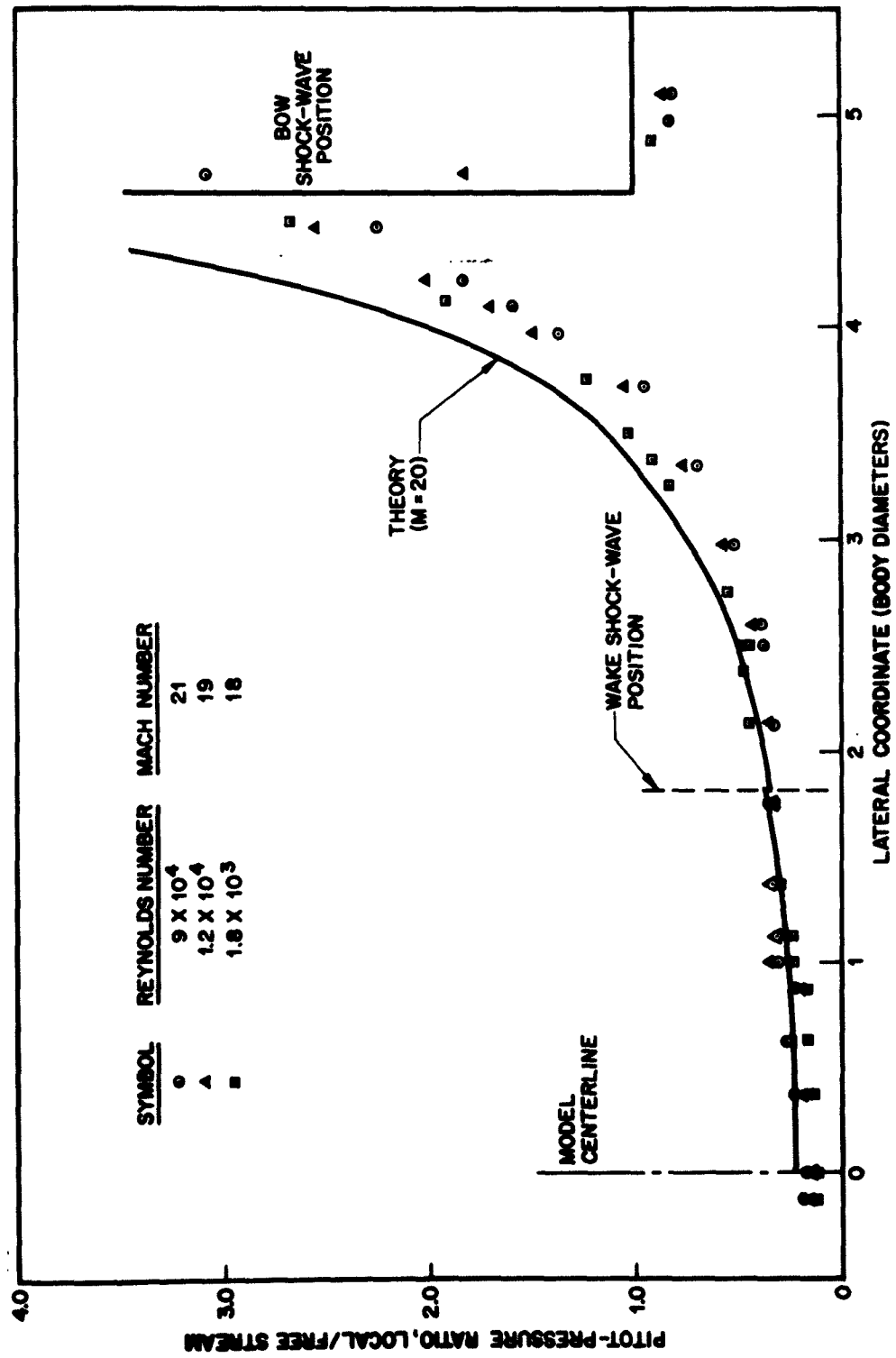


Fig. 6-4 Lateral Pitot-Pressure Distribution (8 Diameters Behind Cylinder)

adverse pressure gradient, and as a result, a fairly wide compression fan is formed. This compression fan finally coalesces into a shock wave at a point sufficiently far downstream that the wave is too weak to be distinguished in pitot-pressure profiles. A second explanation is that the local Knudsen number, based on the pitot-probe diameter, is of the order of unity on the wake centerline at the lowest Reynolds number. For example, at 5 diameters downstream, the local Mach number is calculated to be 2.5 and the Reynolds number, based on probe height, is calculated to be 3.9. The Knudsen number is approximately equal to the ratio of these two numbers. This suggests that the local shock-wave thickness is of the same order as the probe diameter. The interaction between the wave and the probe would therefore be expected to extend over several probe diameters, and no sharp delineation of shock-wave position would be expected. This appears to be especially noticeable at the 5-diameter position.

There is an apparent dependence on the Reynolds number in the nominally inviscid region of the wake, between the wake and bow shock waves. The pressures are consistently higher throughout at the lower Reynolds numbers. This effect is attributable in part to the change in bow shock-wave shape caused by the different effective flow-conicity and real-gas effects at the different Reynolds numbers. At the lowest Reynolds number, as mentioned in the previous section, the bow shock-wave appears to be pushed inward due to the increased tunnel-wall boundary-layer thickness and because of the smaller value of specific heat ratio. However, the effect of lateral displacement alone only accounts for about a quarter of the total difference between the observed pitot pressure and the calculation. It is noted that because of the conical flow, the Mach number immediately outside the bow shock-wave at a given axial station is higher than the value at the model nose, while the static pressure is lower. Both of these factors make the pitot-pressure behind the shock wave smaller than it would be for uniform flow. The effect is particularly noticeable at the 8-diameter position.

Section 7  
PLANNED FUTURE WORK

In general, the computed and measured pressure-distributions and shock-wave shapes are well correlated. It is expected that most of the disparity can be eliminated by making a more refined calculation of the flow field. Effects of the nonperfect gas-flow and conical free-stream, which were intrinsic to the experimental results, are being investigated with a method-of-characteristics that utilizes the thermodynamic properties of equilibrium nitrogen. The improved program will be used to calculate the flow field caused by the cylindrical model for each of the three conditions described in this report.

New instruments are being developed that will measure flow variables other than pressure. A mass-flow probe has yielded promising results in preliminary tests both in the free stream and in the inviscid wake. A total-enthalpy probe has also been tested in the free stream. A tracer-spark technique that measures flow velocity from the displacement of an ionized path during a known interval is also being developed. Measurements from two of these devices, when accompanied by pitot pressure, furnish complete information on the state of a gas in equilibrium. Only when enough quantities are measured can the flow field be determined without reference to assumptions such as those of adiabatic flow or constant total-enthalpy flow.

These new instruments will be used to investigate the flow fields behind various other models. Sharp and blunt-nosed wedges will be used to complete the series of two-dimensional models. The effect of the angle-of-attack upon the viscous wake will be studied. Profiles of pitot pressure, mass flow, and velocity (or total enthalpy) behind these models will give a comprehensive description of the flow fields.

When confidence has been gained in the newly developed instrumentation from tests with two-dimensional models, measurements will be made in the flow field behind axisymmetric models at zero angle-of-attack. Finally, tests of axisymmetric models at angle-of-attack will be conducted.

Section 8  
REFERENCES

1. S. Feldman, "On Trails of Axisymmetric Hypersonic Blunt Bodies Flying Through the Atmosphere," J. Aerospace Sci., Vol. 28, No. 6, Jun 1961, pp. 433-456
2. L. Lees and L. Hromas, "Turbulent Diffusion in the Wake of a Blunt-Nosed Body at Hypersonic Speeds," J. Aerospace Sci., Vol. 29, No. 8, Aug 1962, pp. 976-993
3. H. Lien, J. I. Erdos, and A. J. Pallone, "Nonequilibrium Wakes With Laminar and Turbulent Transport," Preprint 63-447 (paper presented at AIAA Conference on Physics of Entry Into Planetary Atmospheres, MIT, Cambridge, Mass., Aug 1963)
4. L. Lees, "Recent Theoretical Development on Hypersonic Wakes and Trails," Preprint 2662-62 (paper presented at ARS 17th Annual Meeting, Los Angeles, Calif., Nov 1962)
5. Convair, Experimental Study of Hypersonic Turbulent Wakes, by T. A. Dana and W. W. Short, ZPh-103, San Diego, Calif., May 1961
6. R. E. Slattery and W. C. Clay, "The Turbulent Wake of Hypersonic Bodies," Preprint 2673-62 (paper presented at ARS 17th Annual Meeting, Los Angeles, Calif., Nov 1962)
7. A. J. Pallone et al., "Hypersonic Laminar Wakes and Transition Studies," Preprint 63-171 (paper presented at AIAA Summer Meeting, Los Angeles, Calif., Jun 1963)
8. J. F. McCarthy and T. Kubota, "A Study of Wakes Behind a Circular Cylinder at  $M = 5.7$ ," Preprint 63-170 (paper presented at AIAA Summer Meeting, Los Angeles, Calif., Jun 1963)

9. California Institute of Technology, Measurements in Highly Dissipative Regions of Hypersonic Flows. Part II. The Near Wake of a Blunt Body at Hypersonic Speeds (doctoral dissertation), by C. F. Dewey, Pasadena, Calif., Jun 1963
10. J. M. Kendall, "Experimental Study of Sphere and Cylinder Wakes at Supersonic Speeds," Preprint 2677-62 (paper presented at ARS 17th Annual Meeting, Los Angeles, Calif., Nov 1962)
11. Arnold Engineering Development Center, A Miniature Wafer-Style Pressure Transducer, by W. E. Smotherman, AEDC-TR-60-11, Arnold AFS, Tenn., Oct 1960
12. Lockheed Missiles & Space Company, Thermodynamic Properties of Nitrogen, by C. E. Smith, 6-90-62-111, Sunnyvale, Calif., Dec 1962
13. Arnold Engineering Development Center, Some Experiments on Impact-Pressure Probes in a Low Density Hypervelocity Flow, by A. B. Bailey and D. E. Boylan, AEDC-TN-61-161, Arnold AFS, Tenn., Dec 1961
14. G. G. Chernyi, Introduction to Hypersonic Flow, translated and edited by R. F. Probstein, New York, Academic Press, 1961
15. California Institute of Technology, "Correlation of Blunt-Bluff Body Wake Transition Data" (internal memorandum no. 12), by A. Demetriades and H. Gold, Firestone Flight Sciences Laboratory, Pasadena, Calif., 20 Sep 1962
16. National Aeronautics and Space Administration, Supersonic Flow Past a Family of Blunt Axisymmetric Bodies, by M. D. Van Dyke and H. D. Gordon, NASA TR R-1, Moffett Field, Calif., 1959
17. National Aeronautics and Space Administration, Numerical Solutions for Supersonic Flow of an Ideal Gas Around Blunt Two-Dimensional Bodies, by F. B. Fuller, NASA TN D-791, Moffett Field, Calif., Jul 1961
18. National Aeronautics and Space Administration, Comparison of Experimental and Numerical Results for the Flow of a Perfect Gas About Blunt-Nosed Bodies, by M. Inouye and H. Lomax, NASA TN D-1426, Moffett Field, Calif., Sep 1962
19. National Aeronautical Establishment, The Blast Wave Analogy for a Hypersonic Source Flow, by R. F. Meyer, LR-368, Ottawa, Ontario (Canada), Jan 1963